

Application of wavelets to singular integral scattering equations

B. M. Kessler,* G. L. Payne, and W. N. Polyzou

Department of Physics and Astronomy, The University of Iowa, Iowa City, Iowa 52242, USA

(Received 28 June 2004; published 24 September 2004)

The use of orthonormal wavelet basis functions for solving singular integral scattering equations is investigated. It is shown that these basis functions lead to sparse matrix equations which can be solved by iterative techniques. The scaling properties of wavelets are used to derive an efficient method for evaluating the singular integrals. The accuracy and efficiency of the wavelet transforms are demonstrated by solving the two-body T -matrix equation without partial wave projection. The resulting matrix equation which is characteristic of multiparticle integral scattering equations is found to provide an efficient method for obtaining accurate approximate solutions to the integral equation. These results indicate that wavelet transforms may provide a useful tool for studying few-body systems.

DOI: 10.1103/PhysRevC.70.034003

PACS number(s): 21.45.+v, 24.10.-i, 02.60.Nm

I. INTRODUCTION

Few-body systems provide a useful tool for studying the dynamics of hadronic systems. The combination of short-ranged interactions and finite density means that the dynamics of complex hadronic systems can be understood by studying the dynamics of few-degree of freedom subsystems. Few-body systems are simple enough to perform nearly complete high-precision measurements and to perform *ab initio* calculations that are exact to within the experimental precision. This clean connection between theory and experiment has led to an excellent understanding of two-body interactions in low-energy nuclear physics, and a good understanding of the three-body interactions.

Our knowledge of low-energy hadronic dynamics is largely due to the interplay between experimental and computational advances. A complete understanding of even the simplest few-hadron system requires measurements of a complete set of spin observables which have small cross sections and require state of the art detectors. At the same time, the model calculations with realistic interactions are limited by computer speed and memory. In addition the equations are either singular or have complicated boundary conditions which require specialized numerical treatments.

One of the most interesting energy scales is the one where the natural choice of few-body degrees of freedom changes from nucleons and mesons to subnucleon degrees of freedom. The QCD string tension or nucleon size suggests that the relevant scale for the onset of this transition is about a GeV. A consistent dynamics of hadrons or subnuclear particles on this scale must be relativistic; a Galilean invariant theory cannot simultaneously preserve momentum conservation in the lab and center of momentum frames if the initial and final reaction products have different masses. Relativistic dynamical models are most naturally formulated in momentum space. This is due to the presence of momentum-dependent Wigner and/or Melosh rotations as well as square roots that appear in the relationship between energy and momentum.

Nonrelativistic few-body calculations formulated in configuration space with local potentials have the advantage that the matrices obtained after discretizing the dynamical equations are banded, thus reducing the size of the numerical calculations. Equivalent momentum-space calculations lead to dense matrices of comparable dimensions. In addition, the embedding of the two-body interactions in the three-body Hilbert space leads to nonlocalities. Realistic relativistic three-body calculations are just beginning to be solved [1,2]. Numerical methods that can reduce the size of these calculations could make relativistic calculations of realistic systems more tractable.

In this paper we explore the use of wavelet basis functions to reduce the size of momentum space scattering calculations. The resulting linear system can be accurately approximated by a linear system with a sparse kernel. It is our contention that the use of this sparse kernel results in a reduction in the size of the numerical calculation that is comparable to the corresponding configuration space calculations. The advantage is that the wavelet methods can be applied in momentum space and are not limited to local interactions.

The long-term goal is to apply wavelet methods to solve the relativistic three-body problem. In a previous paper [3], we tested this method to solve the nonrelativistic Lippmann-Schwinger equation with a Malfliet Tjon V potential. In this test problem, the s -wave K matrix was computed. The wavelet method led to a significant reduction in the size of the problem. We found that 96% of the matrix elements of the kernel of the integral equation could be eliminated leading to an error of only a few parts in a million.

The success of wavelet method in Ref. [3] suggests that the method should be tested on a more complicated problem. In this paper, we test the wavelet method on the same problem without using partial waves. This leads to a singular two-variable integral equation, which has the same number of continuous variables as the three-body Faddeev equations with partial waves. It is simpler than the full three-body calculation, but is a much larger calculation than was needed in Ref. [3]. In addition, computations that employ conventional methods [4] are available for comparison. In solving this problem it is necessary to address issues involving the storage and computations with large matrices.

*Electronic address: brian-kessler@uiowa.edu

One well-known use of wavelets is in the data compression algorithm used in JPEG files [5]. Our motivation for applying wavelet methods to scattering problems is based on the observation that both a digital photograph and a discretized kernel of an integral equation are two-dimensional arrays of numbers. If wavelets can reduce the size of a digital image, they should have a similar effect on the size of the kernel of an integral equation.

Given the utility of wavelets in digital data processing, it is natural to ask why they have not been used extensively in numerical computations in scattering. One possible reason is because there is a nontrivial learning curve that must be overcome for a successful application to singular integral equations. A relevant feature is that the basis functions have a fractal structure; they are solutions to a linear renormalization group equation and thus have structure on all scales. Numerical techniques that exploit the local smoothness of functions do not work effectively with functions that have structure on all scales.

In Ref. [3], we concluded that these limitations could be overcome by exploiting the renormalization group transformation properties of the basis functions in numerical computations. These equations were used to compute moments of the basis functions with polynomials. These moments were used to construct efficient quadrature methods for evaluating overlap integrals. In addition, these moments could be combined with the renormalization-group equations to perform accurate calculations of the types of singular integrals that appear in scattering problems. A key conclusion of Ref. [3] was that wavelet methods provide an accurate and effective method for solving the scattering equations. In addition, the expected reduction in the size of the numerical problem could be achieved with minimal loss of precision.

There are many kinds of wavelets. In Ref. [3] we found that the Daubechies-3 [6] wavelets proved to be the most useful for our calculations. Numerical methods based on wavelets utilize the existence of two orthogonal bases for a model space. The two bases are related by an orthogonal transformation. The first basis, called the father function basis, samples the data by averaging on small scales. It is the numerical equivalent of a raw digital photograph. The orthogonal transformation is generated by filtering the coefficients of the father function basis into equal numbers of high- and low-frequency parts. The high-frequency parts are associated with another type of basis function known as the mother function. The same filter is again applied only to the remaining low frequency parts, which are divided into high- and low-frequency parts. This is repeated until there is only one low-frequency coefficient. This orthogonal transformation and its inverse can be generated with the same type of efficiency as a fast Fourier transform. The new basis is called the wavelet basis.

For the Daubechies-3 wavelets, both sets of basis functions have compact support. The support of the father function basis functions is small and is determined by the resolution of the model space. The support of the wavelet basis functions is compact, but occurs on all scales between the finest resolution and the coarsest resolution.

The father function for the Daubechies-3 wavelets has the property that a finite linear combination of such functions

can locally pointwise represent a polynomial of degree 2. Integrals over these polynomials and the scaling basis functions can be done exactly and efficiently using a one-point quadrature.

The mother functions have the property that they are orthogonal to polynomials of degree 2. This means that the expansion coefficient for a given mother basis function is zero if the function can be well approximated by a polynomial on the support of the basis function. It is for this reason that most of the kernel matrix elements in this representation are small. Setting these small coefficients to zero is the key approximation that leads to sparse matrices.

Some of the properties that make the Daubechies wavelets interesting for numerical computations are

- the basis functions have compact support,
- the basis functions are orthonormal,
- the basis functions can pointwise represent polynomials of degree 2,
- the wavelet transform automatically identifies the important basis functions,
- there is a simple one-point quadrature rule that is exact for local polynomials of degree 2,
- there are accurate methods for computing the singular integrals of scattering theory,
- the basis functions never have to be computed.

The above list indicates that wavelet bases have many advantages in common with spline bases, which have proven to be very useful in large few-body calculations. Both the spline and wavelet basis functions have compact support, which allows them to efficiently model local structures, both provide pointwise representations of low-degree polynomials, both can be easily integrated using simple quadrature rules, and both can be accurately integrated over the scattering singularity. One feature that distinguishes the wavelet method from the spline method is that the wavelet transform automatically identifies the important basis functions that need to be retained. With splines, the regions that have a lot of structure and require extra splines need to be identified by hand. This is a nontrivial problem in large calculations. The automatic nature of this step is an important advantage of the wavelet method in large calculations. In addition, unlike the spline basis functions, the wavelet basis functions are orthogonal, and the one-point quadrature only requires the evaluation of the driving term or kernel at a single point to compute matrix elements. This leads to numerical approximations that combine the efficiency of the collocation method with the stability of the Galerkin method.

In the next section we give an overview of the properties of wavelets that are used in our numerical computations. Our model problem is defined in Sec. III. The methods of Sec. II are used in Sec. IV to reduce the scattering integral equation in Sec. III to an approximate linear system. The transformation to a sparse-matrix linear system and the methods used to solve the linear equations are discussed in Sec. V. The considerations discussed in this section are important for realistic applications. The results of the model calculations are discussed and compared to the results of partial-wave calculations in Sec. VI. Our conclusions are summarized in Sec. VII. The complex biconjugate gradient algorithm that was used to solve the resulting system of linear equations is outlined in the Appendix.

TABLE I. Scaling coefficients for Daubechies-3 wavelets.

h_0	$(1 + \sqrt{10} + \sqrt{5 + 2\sqrt{10}}) / 16\sqrt{2}$
h_1	$(5 + \sqrt{10} + 3\sqrt{5 + 2\sqrt{10}}) / 16\sqrt{2}$
h_2	$(10 - 2\sqrt{10} + 2\sqrt{5 + 2\sqrt{10}}) / 16\sqrt{2}$
h_3	$(10 - 2\sqrt{10} - 2\sqrt{5 + 2\sqrt{10}}) / 16\sqrt{2}$
h_4	$(5 + \sqrt{10} - 3\sqrt{5 + 2\sqrt{10}}) / 16\sqrt{2}$
h_5	$(1 + \sqrt{10} - \sqrt{5 + 2\sqrt{10}}) / 16\sqrt{2}$

II. WAVELET PROPERTIES

In our work, we use Daubechies' original bases of compactly supported wavelets [6]. In addition to their simplicity, these functions possess many useful properties for numeric calculations, which are discussed at the end of this section.

A. General wavelet analysis

There are two primal basis functions called the father, ϕ , and mother, ψ . The primal father function is defined as the solution of the homogeneous scaling equation

$$\phi(x) = \sqrt{2} \sum_{l=0}^{2K-1} h_l \phi(2x - l), \tag{1}$$

with normalization

$$\int \phi(x) dx = 1. \tag{2}$$

The primal mother function is defined in terms of the father by a similar scaling equation,

$$\psi(x) = \sqrt{2} \sum_{l=0}^{2K-1} g_l \phi(2x - l), \tag{3}$$

where

$$g_l = (-1)^l h_{2K-1-l}. \tag{4}$$

The parameter K is the order of the Daubechies wavelet and the h_l are a unique set of numerical coefficients that satisfy certain relations [6] such as orthogonality of basis functions. We employ wavelets of order $K=3$, henceforth called Daubechies-3 wavelets. The numerical values of the h_l are given in Table I.

Equation (1) is the most important in all of wavelet analysis, as all the properties of a wavelet basis are determined by the so-called filter coefficients h_l . A simple property that follows from the h_l is that the father and mother function both have compact support on the interval $(0, 2K-1)$. All other basis functions are related to the primal father and mother by means of dyadic (power of 2) scale transformations and unit translations,

$$\begin{aligned} \phi_{j,k}(x) &:= 2^{-j/2} \phi(2^j x - k), \\ \psi_{j,k}(x) &:= 2^{-j/2} \psi(2^j x - k). \end{aligned} \tag{5}$$

To solve the two-dimensional integral equation for the T matrix we need to construct a two-dimensional basis in terms

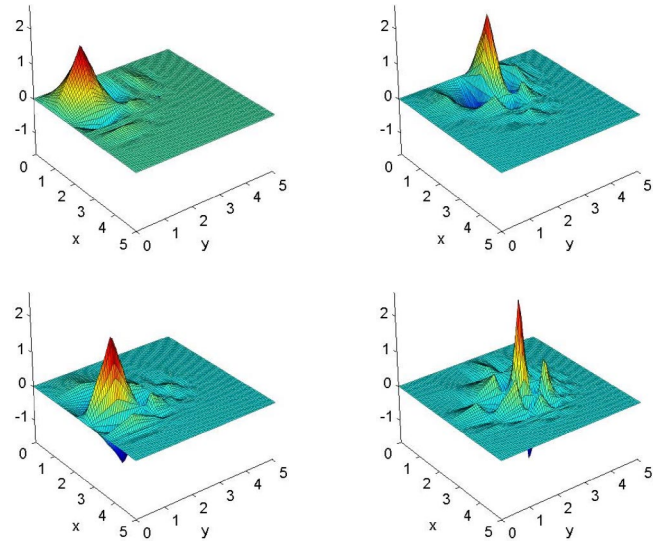


FIG. 1. (Color online) Direct product basis of Daubechies-3 wavelets.

of wavelet functions. The simplest method is to construct a direct-product basis of the one-dimensional functions,

$$\phi_{m,l}(x)\phi_{n,k}(y), \quad \phi_{m,l}(x)\psi_{n,k}(y),$$

$$\psi_{m,l}(x)\phi_{n,k}(y), \quad \text{and} \quad \psi_{m,l}(x)\psi_{n,k}(y). \tag{6}$$

The primal versions of these four basis function types for the Daubechies-3 wavelets are shown in Fig. 1. The complex pointwise structure of the basis functions tends to obscure their ability to accurately and efficiently represent smooth functions. Fortunately, the pointwise structure never appears in calculations, since all calculations are made in terms of the simple scaling equation (1).

B. Equivalent representations and wavelet transforms

If one includes wavelets of all scales, then one can obtain a basis for $L^2(\mathbb{R})$. In practice however, one chooses a fine approximation scale J and constructs an approximation basis with respect to this scale. At any scale, there are two equivalent bases in terms of wavelet functions. The first basis consists of translates of the father function on the finest scale J . The second basis consists of the father functions on the coarsest scale $j=0$ and mother functions on all intermediate scales $j=0, \dots, J-1$. So, for any function we have two equivalent approximations given by

$$f(x) = \sum_l a_l \phi_{J,l}(x) = \sum_l a'_l \phi_{0,l}(x) + \sum_{j=0}^{J-1} \sum_l d_{j,l} \psi_{j,l}(x). \tag{7}$$

In two dimensions, the two equivalent representations are given by the direct product of the one-dimensional representations, which gives us the four types of basis functions in Eq. (6). It turns out that the first representation is typically dense while the second can often be truncated to a sparse representation by eliminating expansion coefficients with a magnitude below some certain threshold. This is because the

father functions can exactly represent polynomials of degree $K-1$ while the mother functions are orthogonal to such polynomials [6]. Specifically,

$$\int x^k \psi(x) dx = 0, \quad 0 \leq k \leq K-1. \quad (8)$$

Thus for any function that is well-represented by low degree polynomials on the scale J , most of the coefficients $d_{j,l}$ in the second representation will be small. These small coefficients can be eliminated with a local error of $O(\epsilon)$, where ϵ is the threshold of the truncation. A fast orthogonal transformation known as the discrete wavelet transform [7] links the two bases given above. This allows us to compute projections in the first basis where the single scale and single type of basis function make the approximations accurate and efficient. Then we can apply the discrete wavelet transform to quickly produce the sparse basis, which is useful for solving linear systems.

C. Application of the scaling equation

Now, we briefly discuss some of the useful results that follow from the scaling equation (1). For a more detailed treatment see Refs. [3,8]. First we consider the moments of the father function defined by

$$\langle x^k \rangle := \int x^k \phi(x) dx. \quad (9)$$

Applying the scaling equation (1) to Eq. (9) gives

$$\langle x^k \rangle = \frac{1}{2^k} \sum_l \frac{h_l}{\sqrt{2}} \sum_{m=0}^k \binom{k}{m} l^{k-m} \langle x^m \rangle. \quad (10)$$

This recursion relation, along with the normalization condition, $\langle x^0 \rangle := 1$, can be used to compute all of the moments of the father function in terms of the filter coefficients h_l . These moments can be used to construct quadrature rules, which are used to approximate the projection of an arbitrary function $f(x)$ onto a wavelet basis. We employ the simplest such quadrature, the one-point quadrature [9]. This quadrature is based on the identity $\langle x^2 \rangle = \langle x \rangle^2$ and results in a local error of $O(f^{(3)}(x))$.

It is also important in applications to consider the case where the interval of integration is finite. Specifically, we consider integrals over left-hand and right-hand end points of the form [10]

$$\begin{aligned} \langle x^k \rangle_m^+ &:= \int_0^\infty \phi(x-m) x^k dx, \\ \langle x^k \rangle_m^- &:= \int_{-\infty}^0 \phi(x-m) x^k dx, \end{aligned} \quad (11)$$

and

$$\begin{aligned} \Delta_{mn}^+ &:= \int_0^\infty \phi(x-m) \phi(x-n) dx, \\ \Delta_{mn}^- &:= \int_{-\infty}^0 \phi(x-m) \phi(x-n) dx. \end{aligned} \quad (12)$$

Applying the scaling equation (1) to these integrals gives linear relations such as

$$\langle x^k \rangle_m^+ = 2^{-k-1/2} \sum_{l=0}^{2K-1} h_l \langle x^k \rangle_{2m+l}^+ \quad (13)$$

and

$$\Delta_{m,n}^+ = \sum_{r=0}^{2K-1} \sum_{s=0}^{2K-1} h_r h_s \Delta_{2m+r, 2n+s}^+. \quad (14)$$

These linear systems can be solved for the cases of $m, n = -1, -2, \dots, -(2K-2)$ using the previously computed moments for $\langle x^k \rangle_m^+$ and the orthogonality relations for $\Delta_{m,n}^+$.

In Ref. [3], we introduced a method for computing singular integrals of the form

$$S_k := \int \frac{\phi(x-k)}{x+i0^+} dx, \quad (15)$$

where 0^+ is a positive infinitesimal quantity. Applying the scaling equation (1) gives the degenerate linear relations

$$S_k = \sqrt{2} \sum_{l=0}^{2K-1} h_l S_{2k-l}. \quad (16)$$

These can be supplemented with a normalization condition

$$-i\pi = \int_{-a}^a \frac{dx}{x+i0^+} = \sum_n \int_{-a}^a \phi(x-n) \frac{dx}{x+i0^+} = \sum_n S_{n,a}, \quad (17)$$

which follows from the identity $1 = \sum_n \phi(x-n)$. Finally, we need the nonsingular integrals which can be obtained using the recursion relation (16) and the convergent expansion for large n given by

$$\begin{aligned} S_{n,a} &= \int_{-a}^a \frac{\phi(x-n)}{x+i0^+} dx = \frac{1}{n} \int_{-a-n}^{a-n} \frac{\phi(y)}{1+y/n} dy \\ &= \frac{1}{n} \sum_{k=0}^{\infty} \left(\frac{-1}{n} \right)^k \int_{-a-n}^{a-n} \phi(y) y^k dy, \end{aligned} \quad (18)$$

where the final integrals can be calculated using the methods for Eqs. (9) and (11). The values of the singular integrals are given in Table II.

For a more thorough and detailed discussion of these calculations and additional properties of wavelets see Refs. [3,8].

III. TWO-BODY T MATRIX IN MOMENTUM SPACE

The two-body T matrix is given by the solution to the Lippmann-Schwinger equation

TABLE II. Integrals over singularity.

S_{-1}	-0.1717835441734	-i 4.041140804162
S_{-2}	-1.7516314066967	+i 1.212142562305
S_{-3}	-0.3025942645356	-i 0.299291822651
S_{-4}	-0.3076858066180	-i 0.013302589081

$$T = V + VG_0T, \quad (19)$$

where V is the two-body potential and $G_0 = (E + i\epsilon - H_0)^{-1}$ is the free two-body propagator. In momentum space, this equation becomes

$$v(p', p, x', x) = \frac{1}{\pi} \left[\frac{\lambda_R}{\sqrt{(p'^2 + p^2 - 2p'px'x + \mu_R)^2 - 4p'^2p^2(1-x'^2)(1-x^2)}} - \frac{\lambda_A}{\sqrt{(p'^2 + p^2 - 2p'px'x + \mu_A)^2 - 4p'^2p^2(1-x'^2)(1-x^2)}} \right]. \quad (21)$$

The parameters for this potential are: $\lambda_A = 626.8932$ MeV fm, $\mu_A = 1.55$ fm $^{-1}$, $\lambda_R = 1438.723$ MeV fm, $\mu_R = 3.11$ fm $^{-1}$, which correspond to those used in Ref. [4]. We use a nucleon mass such that $1/m = 41.47$ MeV fm 2 .

In our work, we consider solutions for the half off-shell T matrix, $T(p', p_0, x')$. Traditionally, the T matrix is decomposed in a partial wave basis using

$$T(p', p_0, x') = \sum_{l=0}^{\infty} \frac{2l+1}{4\pi} T_l(p') P_l(x'), \quad (22)$$

where the P_l are Legendre polynomials. Each amplitude $T_l(p')$ must be solved for individually. For high energies, a significant number of amplitudes may need to be included to ensure convergence [4].

The magnitude squared of the on-shell T matrix is proportional to the differential cross section. Furthermore, the on-shell partial wave amplitudes $T_l(p_0)$ can be parametrized as

$$T_l(p_0) = -\frac{2}{\pi} \frac{1}{mp_0} e^{i\delta_l(p_0)} \sin(\delta_l(p_0)), \quad (23)$$

where the $\delta_l(p_0)$ are experimentally determined phase shifts. These phase shifts are used to fit realistic nucleon-nucleon potentials and should be accurately reproduced by any viable solution method.

IV. WAVELET REPRESENTATION

To solve Eq. (20) we need to transform the half interval $[0, \infty)$ corresponding to the momentum variable into a finite interval $[-a, b]$. For computational convenience we also

$$T(p', p, x') = \frac{1}{2\pi} v(p', p, x', 1) - m \int_0^{\infty} dp'' p''^2 \int_{-1}^1 dx'' \times v(p', p'', x', x'') \frac{1}{p''^2 - p_0^2 - i\epsilon} T(p'', p, x''), \quad (20)$$

where m is the mass of the particles, p_0 is the on-shell momentum, $x' = \hat{\mathbf{p}}' \cdot \hat{\mathbf{p}}$, $x'' = \hat{\mathbf{p}}'' \cdot \hat{\mathbf{p}}$, and v is the two-body potential with the azimuthal angle dependence integrated out. For our calculations, we use a Malfiet-Tjon III potential [11] with attractive and repulsive parts. In this case, the azimuthal integration can be carried out analytically giving

transform the interval $[-1, 1]$ associated with the angular variable into the region $[-c, d]$. For the first transformation we use the following map:

$$p(k) := p_0 \frac{b a + k}{a b - k}, \quad k(p) := \frac{ab(p - p_0)}{ap + p_0 b}, \quad (24)$$

which maps the scattering singularity at $p'' = p_0$ to the origin. Then we have

$$dp = p_0 \frac{b(b+a)}{a(b-k)^2} dk \quad (25)$$

and

$$\frac{1}{p - p_0} = \frac{a(b-k)}{(a+b)p_0 k}. \quad (26)$$

The second mapping is the simple linear transformation

$$x(u) := \frac{2u - d + c}{d + c}, \quad u(x) := \frac{(d+c)x + (d-c)}{2}, \quad (27)$$

which gives

$$dx = \frac{2}{d+c} du. \quad (28)$$

We now apply these maps to Eq. (20) to obtain an equivalent integral equation on the rectangular region $[-a, b] \times [-c, d]$. For notational convenience we define

$$\begin{aligned}
 f(p', x') &:= T(p', p_0, x'), \\
 g(p', x') &:= \frac{1}{\pi} v(p', p_0, x', 1),
 \end{aligned} \tag{29}$$

and for the nonsingular part of the kernel

$$L(p', p'', x', x'') := m \frac{v(p', p'', x', x'') p''^2}{p'' + p_0}. \tag{30}$$

Now, we let

$$\begin{aligned}
 \tilde{f}(k', u') &:= f(p(k'), x(u')), \\
 \tilde{g}(k', u') &:= g(p(k'), x(u')),
 \end{aligned} \tag{31}$$

and

$$\tilde{L}(k', k'', u', u'') := L(p(k'), p(k''), x(u'), x(u'')) \frac{2}{d+c} \frac{b}{b-k''}. \tag{32}$$

The last factor in this equation comes from applying Eqs. (25), (26), and (28), which gives

$$\frac{1}{p'' - p_0} dp'' dx'' = \frac{1}{k''} \frac{2}{d+c} \frac{b}{b-k''} dk'' du''. \tag{33}$$

Finally, substituting Eqs. (31) and (32) into Eq. (20) gives

$$\tilde{f}(k', u') = \tilde{g}(k', u') - \int_{-a}^b dk'' \int_{-c}^d du'' \frac{\tilde{L}(k', k'', u', u'')}{k''} \tilde{f}(k'', u''). \tag{34}$$

Now, we project this equation onto the wavelet basis which results in a Galerkin-type procedure. In general, one can choose a separate fine scale in each variable. For notational simplicity, we will consider the case where $J_k = J_u = J$. In this case, we approximate \tilde{f} using

$$\tilde{f}(k', u') \approx \sum_{m,n} \tilde{f}_{m,n} \phi_{J,m}(k') \phi_{J,n}(u'). \tag{35}$$

Substituting this in Eq. (34) and multiplying by $\phi_{J,m'}(k') \phi_{J,n'}(u')$ and integrating over k' and u' gives the linear equation

$$\begin{aligned}
 \sum_{m,n} N_{m',n';m,n} \tilde{f}_{m,n} &= \tilde{g}_{m',n'} - \sum_{m,n} \int_{-a}^b dk' \int_{-c}^d du' \\
 &\times \int_{-a}^b dk'' \int_{-c}^d du'' \phi_{J,m'}(k') \phi_{J,n'}(u') \\
 &\times \frac{\tilde{L}(k', k'', u', u'')}{k''} \phi_{J,m}(k'') \phi_{J,n}(u'') \tilde{f}_{m,n},
 \end{aligned} \tag{36}$$

where

$$\tilde{g}_{m',n'} := \int_{-a}^b dk' \int_{-c}^d du' \tilde{g}(k', u') \phi_{J,m'}(k') \phi_{J,n'}(u') \tag{37}$$

and

$$\begin{aligned}
 N_{m',n';m,n} &:= \int_{-a}^b dk' \int_{-c}^d du' \phi_{J,m'}(k') \\
 &\times \phi_{J,n'}(u') \phi_{J,m}(k') \phi_{J,n}(u').
 \end{aligned} \tag{38}$$

We can evaluate $\tilde{g}_{m',n'}$ using the one-point quadrature [10] discussed earlier and an end-point quadrature based on the partial moments [3]. $N_{m',n';m,n}$ is simply the direct product of block diagonal matrices consisting of identity blocks and blocks of the form Δ^\pm given in Eq. (12). The final term in Eq. (36) can be evaluated using the subtraction

$$\begin{aligned}
 \tilde{L}_{m',n';m,n} &:= \int_{-a}^b dk' \int_{-c}^d du' \int_{-a}^b dk'' \int_{-c}^d du'' \phi_{J,m'}(k') \phi_{J,n'}(u') \\
 &\times \frac{\tilde{L}(k', k'', u', u'')}{k''} \phi_{J,m}(k'') \phi_{J,n}(u'') \\
 &= \int_{-a}^b dk' \int_{-c}^d du' \int_{-a}^b dk'' \int_{-c}^d du'' \phi_{J,m'}(k') \phi_{J,n'}(u') \\
 &\times \frac{\tilde{L}(k', k'', u', u'') - \tilde{L}(k', 0, u', u'')}{k''} \phi_{J,m}(k'') \phi_{J,n}(u'') \\
 &+ \int_{-a}^b dk' \int_{-c}^d du' \int_{-c}^d du'' \phi_{J,m'}(k') \phi_{J,n'}(u') \\
 &\times \tilde{L}(k', 0, u', u'') \phi_{J,n}(u'') \int_{-a}^b \frac{\phi_{J,m}(k'')}{k''} dk''.
 \end{aligned} \tag{39}$$

The first term in this equation is nonsingular and can be approximated using the quadrature methods previously discussed. Likewise, the k', u'', u' integrations in the second term can be carried out in the same manner. The final integration over k'' can be accomplished using the method following Eq. (16).

Thus, the problem is reduced to solving a linear system of the form

$$\sum_{m,n} (N_{m',n';m,n} + \tilde{L}_{m',n';m,n}) \tilde{f}_{m,n} = \tilde{g}_{m',n'}. \tag{40}$$

Once we have solved this equation for $\tilde{f}_{m,n}$ we can substitute this approximate solution back into the right-hand side of the original equation to obtain a refined solution.

V. WAVELET TRANSFORM AND SPARSE SOLUTION

The eigenvalues of Δ^+ accumulate at 0 while those of Δ^- accumulate at 1 as K increases [12]. This makes the matrix \mathbf{N} , and consequently the right-hand side of Eq. (40), numerically ill behaved. To circumvent this difficulty we can precondition the system by inverting \mathbf{N} , which is easily accomplished by inverting the two blocks Δ^+ and Δ^- and using the direct product structure of \mathbf{N} . If we define

$$\mathbf{h} = \mathbf{N}\tilde{\mathbf{f}}, \quad (41)$$

then Eq. (40) becomes

$$(\mathbf{I} + \mathbf{L}\mathbf{N}^{-1})\mathbf{h} = \tilde{\mathbf{g}}. \quad (42)$$

If we define

$$\mathbf{A} = (\mathbf{I} + \mathbf{L}\mathbf{N}^{-1}), \quad (43)$$

then Eq. (42) is a simply linear system of the form

$$\mathbf{A}\mathbf{h} = \tilde{\mathbf{g}}. \quad (44)$$

This is a large dense linear system. However, as shown in Eq. (7), there are two equivalent representations that are linked by a fast orthogonal transformation. In two variables, the matrix representation of this transformation is simply the direct product of the one-dimensional transformation matrices that are given in many standard references [7]. If we denote this matrix as \mathbf{W} then we can transform Eq. (44) as

$$(\mathbf{W}\mathbf{A}\mathbf{W}^T)\mathbf{W}\mathbf{h} = \mathbf{W}\tilde{\mathbf{g}}. \quad (45)$$

Now we make the definitions

$$\hat{\mathbf{A}} = \mathbf{W}\mathbf{A}\mathbf{W}^T, \quad \hat{\mathbf{h}} = \mathbf{W}\mathbf{h}, \quad \hat{\mathbf{g}} = \mathbf{W}\tilde{\mathbf{g}}. \quad (46)$$

Then as mentioned in reference to Eq. (7) we can truncate the matrix $\hat{\mathbf{A}}$ by eliminating all elements with a magnitude below some certain threshold ϵ , where the error introduced is proportional to ϵ . The matrix $\hat{\mathbf{A}}$ can be stored in a sparse format such as compressed column format (CCS) [13], which permits both efficient storage and matrix multiplication. These savings help eliminate computationally costly writing and reading from the hard disk when solving the linear system.

To solve the sparse system we use the complex biconjugate gradient method [7,14] which we present for general complex matrices in the Appendix. This method is a simple and effective iterative method for general sparse matrices. In addition, this method, like all iterative techniques, is readily amenable to parallel processing of the matrix multiplication. Once the solution to Eq. (45) is found, it is a simple matter to recover $\tilde{\mathbf{f}}$ by applying the inverse transform \mathbf{W}^T and the inverse matrix \mathbf{N}^{-1} . In particular,

$$\tilde{\mathbf{f}} = \mathbf{N}^{-1}\mathbf{W}^T\hat{\mathbf{h}}. \quad (47)$$

VI. RESULTS AND ANALYSIS

We made calculations using the Daubechies-3 wavelets at scales up to $J=5$ in each variable. The total number of wavelet basis functions in each variable was taken to be 2^M , where $M=J+2$. If we take $a=c=1$, then b and d are determined by

$$\begin{aligned} b &= 2^{-J_k}[2^{M_k} - (2K - 2)] - a, \\ d &= 2^{-J_u}[2^{M_u} - (2K - 2)] - c. \end{aligned} \quad (48)$$

Using these parameters calculations were performed at lab energies of 300 and 800 MeV to test the efficacy of the

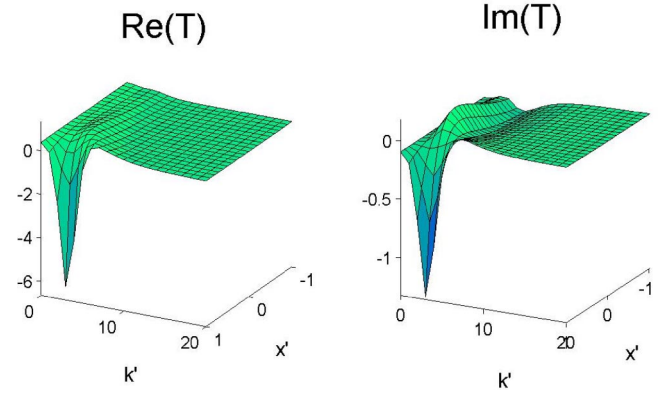


FIG. 2. (Color online) Half off-shell T matrix at 800 MeV.

method in different energy regimes. Figure 2 shows the real and imaginary parts of the half off-shell T matrix as a function of momentum p' and the scattering angle $x' = \cos(\theta)$ at a scattering energy of 800 MeV. Daubechies-3 wavelets were used with $M_k = M_u = 5$.

It can be seen that the real part of the T matrix is relatively smooth, while the imaginary part does have some structure. The fact that the T matrix is smooth with isolated structure suggests that wavelet methods should be able to efficiently compress the matrix $\hat{\mathbf{A}}$. Figure 3 shows the on-shell T matrix as a function of angle $x' = \cos(\theta)$ at a scattering energy of 300 MeV. These calculations were made using Daubechies-3 wavelets with $M_k = M_u = 5$.

From these graphs the general smoothness of the on-shell amplitude is apparent. We can also see the forward peaking of the scattering amplitude that is expected at higher energies.

From a numerical standpoint, the first aspect of the calculation to consider is the general convergence of the method as the number of basis functions is increased. Tables III and IV illustrate the convergence of the method as the number of basis functions is increased. The quoted values are for on-shell scattering at an angle of 90° using Daubechies-3 wavelets with no truncation. From Table III, we see that the majority of improvement occurs as M_k is increased. This can be attributed to the fact that the integral over k'' in the kernel is singular and thus requires more basis functions to accurately represent the dependence on this variable.

All of these calculations were made by solving the linear system (42). It is instructive to consider the behavior if one

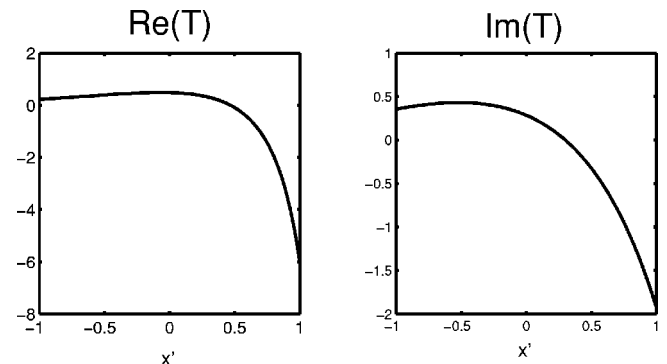


FIG. 3. On-shell T matrix at 300 MeV.

TABLE III. Convergence as a function of total number of basis functions: 300 MeV.

M_k	M_u	$\text{Re}(T(p_0, p_0, 0))$	$\text{Im}(T(p_0, p_0, 0))$
4	4	0.484065410	0.292438234
4	5	0.483906981	0.293504057
5	4	0.491111143	0.286418162
5	5	0.490972783	0.287464852
5	6	0.490891484	0.287452418
6	5	0.491773044	0.286276262
6	6	0.491691220	0.286263888
6	7	0.491678773	0.286256958
7	6	0.491772680	0.286123199
7	7	0.491760404	0.286116271

attempts to solve Eq. (40) using iterative methods without directly inverting \mathbf{N} first. Table V compares the error in the residual, $e_n = \|\hat{\mathbf{r}}_n\| = \|\hat{\mathbf{g}} - \hat{\mathbf{A}}\hat{\mathbf{h}}_n\|$, as a function of the number of iterations. As the number of iterations n is increased the preconditioned method converges very rapidly, while the non-preconditioned method fails to converge adequately.

Now we turn our attention to the compression of the sparse matrix and its subsequent effect on the calculation. Figure 4 displays such a representation for scattering at 800 MeV using Daubechies-3 wavelets with $M_k=4$, $M_u=3$. The plot shows the location of the nonzero elements of $\hat{\mathbf{A}}$ after it has been truncated at the threshold level $\epsilon=10^{-5}$. This threshold produces a matrix with 19% of the elements of the full matrix. The ordering scheme for $\hat{\mathbf{A}}$ used in the plot places the elements associated with finer scales at higher indices. The degree of sparsity increases considerably as the scale increases, which demonstrates that less and less elements are needed at finer scales.

A key advantage of wavelets is that this reduction in the number of nonzero matrix elements significantly reduces the time required to solve the linear system. For the biconjugate gradient method, each iteration requires two matrix multiplications, which take a time proportional to the number of nonzero elements in the matrix. Thus a reduction in the num-

TABLE IV. Convergence as a function of total number of basis functions: 800 MeV.

M_k	M_u	$\text{Re}(T(p_0, p_0, 0))$	$\text{Im}(T(p_0, p_0, 0))$
4	4	0.456127838	0.126626540
4	5	0.454750689	0.126515462
5	4	0.456227507	0.113862313
5	5	0.455006434	0.113967425
5	6	0.454697067	0.113367584
6	5	0.455242066	0.111684819
6	6	0.454931562	0.111107815
6	7	0.454884387	0.111005571
7	6	0.454978565	0.110889988
7	7	0.454931334	0.110788571

TABLE V. Convergence of the biconjugate gradient method.

n	e_n (nonpreconditioned)	e_n (preconditioned)
10	3.25×10^{-4}	1.98×10^{-3}
20	4.21×10^{-4}	3.07×10^{-5}
30	7.23×10^{-5}	2.03×10^{-6}
40	9.94×10^{-4}	9.10×10^{-10}
50	1.01×10^{-4}	8.09×10^{-13}

ber of nonzero elements reduces the solution time by a corresponding amount. The other major source of computational effort is setting up and storing the various matrices used in the problem. For the range of test cases we considered, the solution of the sparse linear systems only took 5–10 % of the total computational time. Other methods, such as those based on splines, will have comparable setup time, but longer solution time for the corresponding dense linear system.

In Table VI, the effect of truncating the matrix $\hat{\mathbf{A}}$ on the convergence of the solution is illustrated for various threshold levels with a lab energy of 800 MeV. This calculation was performed using the Daubechies-3 wavelets with $M_k = M_u = 6$. Comparing these results with those in Table III, we see that even keeping just one percent of the matrix elements we are able to reproduce the T matrix to the same precision as the accuracy of the untruncated matrix.

Finally, we consider the accuracy of the phase shifts determined by our momentum vector approach. To calculate the phase shifts we project our T matrix onto the partial waves using

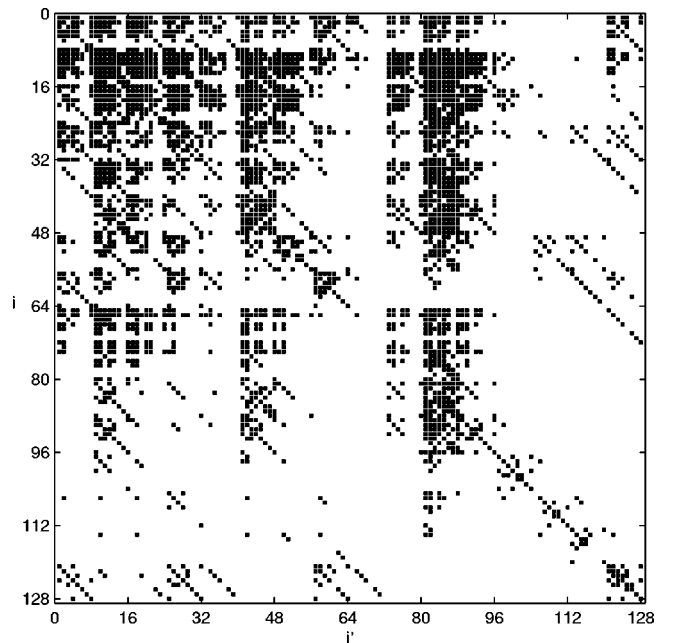

 FIG. 4. Location of the nonzero of elements of $\hat{\mathbf{A}}$.

TABLE VI. Effect of truncation on the on-shell T matrix at 800 MeV for scattering at 180° , 90° , and 0° corresponding to $T(p_0, p_0, -1)$, $T(p_0, p_0, 0)$, and $T(p_0, p_0, +1)$.

ϵ	%	$\text{Re}(T(p_0, p_0, -1))$	$\text{Im}(T(p_0, p_0, -1))$
0	100	0.249235	-0.0777091
10^{-8}	23	0.249235	-0.0777093
10^{-7}	14	0.249234	-0.0777116
10^{-6}	8	0.249217	-0.0777525
10^{-5}	1	0.248296	-0.0770660
ϵ	%	$\text{Re}(T(p_0, p_0, 0))$	$\text{Im}(T(p_0, p_0, 0))$
0	100	0.454932	0.111108
10^{-8}	23	0.454932	0.111108
10^{-7}	14	0.454932	0.111108
10^{-6}	8	0.454941	0.111117
10^{-5}	1	0.454966	0.111154
ϵ	%	$\text{Re}(T(p_0, p_0, +1))$	$\text{Im}(T(p_0, p_0, +1))$
0	100	-6.16347	-1.31548
10^{-8}	23	-6.16347	-1.31548
10^{-7}	14	-6.16347	-1.31548
10^{-6}	8	-6.16346	-1.31548
10^{-5}	1	-6.16327	-1.31559

$$T_l(p') = 2\pi \int_{-1}^1 P_l(x') T(p', p_0, x') dx'. \quad (49)$$

We compute the integrals using 20 Gauss-Legendre points [15]. From the T_l it is straightforward to calculate the phase shifts using Eq. (23). Table VII displays these phase shifts (calculated for $E_{\text{Lab}}=800$ MeV using Daubechies-3 wavelets with $M_k=M_u=7$ and truncating all but 2% of the coeffi-

TABLE VII. Comparison of 800-MeV phase shifts with standard methods.

l	$\delta_l(p_0)$ (standard)	$\delta_l(p_0)$ (wavelet)
0	-0.2535	-0.2534
1	0.2950	0.2949
2	0.3635	0.3634
3	0.2747	0.2746
4	0.1755	0.1755
5	0.1053	0.1052
6	0.06169	0.06168
7	0.03591	0.03591
8	0.02089	0.02089
9	0.01217	0.01217
10	0.007110	0.007109
11	0.004164	0.004163
12	0.002445	0.002444
13	0.001439	0.001437

icients) compared with phase shifts calculated using standard partial wave techniques. The agreement between the two methods is very good for all the phase shifts.

VII. CONCLUSIONS

We have shown that it is possible to use wavelets to calculate the two-body scattering matrix in terms of momentum vectors without resorting to partial waves. We were able to accurately reproduce the phase shifts of the Malfliet-Tjon potential. These calculations lead to sparse matrices, which can be efficiently inverted using standard iterative methods. Application of a simple preconditioning matrix was shown to be necessary to achieve convergence of the iterative methods. Traditional methods for solving scattering equations in momentum space typically produce dense matrices that require a large amount of storage and are time consuming to invert. These are promising results because relativistic scattering equations are naturally formulated in momentum space. Also, the scattering boundary conditions are most easily treated in momentum space. Wavelet methods can help treat both of these problems.

One of the main advantages of wavelet methods over methods such as splines is that the wavelet transform presents a method that automatically determines what basis functions are necessary for a given accuracy. Unfortunately, this also leads to one of the main drawbacks of this method. In our procedure, a large dense matrix \mathbf{A} needs to be produced first and then this is transformed to a sparse matrix. Most of the computational time is spent constructing and transforming this matrix into a sparse format. The subsequent solution of the sparse linear system takes relatively little computational effort.

For this specific problem, wavelet methods based on momentum vectors may not be necessary. The maximum number of partial waves that needs to be included to achieve convergence, $l_{\text{max}}=14$ [4], is simply too small to gain a computational benefit from using wavelets in the angular variable. To achieve a computational benefit we should use less basis functions in the angular variable than the maximum number of partial waves. In the three-body problem or at much higher energies, the number of partial waves that need to be included increases considerably and computational benefits may be gained from employing a momentum vector approach.

ACKNOWLEDGMENTS

This work was supported in part by the U.S. Department of Energy, under Contract No. DE-FG02-86ER40286.

APPENDIX: COMPLEX BICONJUGATE GRADIENT METHOD

The biconjugate gradient method [7,14] is an iterative technique for solving large matrix equations of the form

$$\mathbf{Ax} = \mathbf{b}.$$

The advantage of this method for large sparse matrices is that it only involves matrix multiplication by \mathbf{A} and its adjoint,

both of which can be accomplished efficiently in a sparse storage format such as CCS [13]. The algorithm generates a sequence of approximate solutions, \mathbf{x}_k with residual $\mathbf{r}_k = \mathbf{b} - \mathbf{A}\mathbf{x}_k$. One iterates until the norm of the residual is less than some predetermined value.

This method is traditionally formulated for real matrices, but the extension to complex matrices is straightforward. Below we present the algorithm for general complex matrices. For our calculations, we start with the initial approximate solution

$$\mathbf{x}_0 = \mathbf{b}$$

with the residual

$$\mathbf{r}_0 = \mathbf{b} - \mathbf{A}\mathbf{x}_0.$$

For the initial values of the bi-residual $\bar{\mathbf{r}}_0$, the direction vector \mathbf{p}_0 , and bi-direction $\bar{\mathbf{p}}_0$ we use

$$\bar{\mathbf{r}}_0 = \mathbf{b} - \mathbf{A}^\dagger \mathbf{x}_0,$$

$$\mathbf{p}_1 = \mathbf{r}_0,$$

$$\bar{\mathbf{p}}_1 = \bar{\mathbf{r}}_0.$$

Then we use the recurrence relations

$$\alpha_k = \frac{\bar{\mathbf{r}}_{k-1}^\dagger \mathbf{r}_{k-1}}{\bar{\mathbf{p}}_k^\dagger \mathbf{A} \mathbf{p}_k},$$

$$\mathbf{x}_k = \mathbf{x}_{k-1} + \alpha_k \mathbf{p}_k,$$

$$\mathbf{r}_k = \mathbf{r}_{k-1} - \alpha_k \mathbf{A} \mathbf{p}_k,$$

$$\bar{\mathbf{r}}_k = \bar{\mathbf{r}}_{k-1} - \alpha_k^* \mathbf{A}^\dagger \bar{\mathbf{p}}_k,$$

$$\beta_k = \frac{\bar{\mathbf{r}}_k^\dagger \mathbf{r}_k}{\bar{\mathbf{r}}_{k-1}^\dagger \mathbf{r}_{k-1}},$$

$$\mathbf{p}_{k+1} = \mathbf{r}_k + \beta_k \mathbf{p}_k,$$

$$\bar{\mathbf{p}}_{k+1} = \bar{\mathbf{r}}_k + \beta_k^* \bar{\mathbf{p}}_k$$

to generate an improved approximation. This is repeated until the desired accuracy is obtained. We measure the accuracy by the $\ell^2(\mathbb{C})$ norm of the residual.

-
- [1] A. Stadler and F. Gross, Phys. Rev. Lett. **78**, 26 (1997).
 - [2] H. Kamada, W. Glöckle, J. Golak, and Ch. Elster, Phys. Rev. C **66**, 044010 (2002).
 - [3] B. M. Kessler, G. L. Payne, and W. N. Polyzou, Few-Body Syst. **33**, 1 (2003); Nucl. Phys. **A737CF**, S311 (2004).
 - [4] Ch. Elster, J. H. Thomas, and W. Glöckle, Few-Body Syst. **24**, 55 (1998).
 - [5] <http://www.jpeg.org/demo/FAQJpeg2k/index.htm>
 - [6] Ingrid Daubechies, Commun. Pure Appl. Math. **41**, 909 (1988).
 - [7] W. H. Press, S. A. Teukolsky, W. T. Vettering, and B. P. Flannery, *Numerical Recipes in C* (University Press, Cambridge, England, 1992).
 - [8] B. M. Kessler, G. L. Payne, and W. N. Polyzou, nucl-th/0305025.
 - [9] W. Sweldens and R. Piessens, SIAM (Soc. Ind. Appl. Math.) J. Numer. Anal. **31**, 1240 (1994).
 - [10] W.-C. Shann, in *Proceedings for the 1993 Annual Meeting of Chinese Mathematics Association*. Chiao-Tung Univ., (1993); W.-C. Shann and J.-C. Yan, Technical Report 9301, Department of Mathematics, National Central University (1993), <http://www.math.ncu.edu.tw/~shann/Math/pre.html>
 - [11] R. A. Malfliet and J. A. Tjon, Nucl. Phys. **A127**, 161 (1969).
 - [12] B. M. Kessler, J. W. Van Orden, and F. Gross, JLAB internal publication (2003).
 - [13] R. Barret *et al.*, *Templates for the Solution of Linear Systems: Building Blocks for Iterative Methods* (SIAM, Philadelphia, 1994), http://www.netlib.org/linalg/html_templates/report.html
 - [14] G. H. Golub and C. F. Van Loan, *Matrix Computations* (Johns Hopkins University Press, Baltimore, 1996).
 - [15] M. Abramowitz and I. A. Stegun, *Handbook of Mathematical Functions* (Dover, New York, 1970).